

Investigating the Relative Gas and Small Dust Grain Surface Heights in Protoplanetary Disks

Evan A. Rich¹®, Richard Teague²®, John D. Monnier¹®, Claire L. Davies³®, Arthur Bosman¹®, Tim J. Harries³®, Nuria Calvet¹®, Fred C. Adams¹,⁴®, David Wilner²®, and Zhaohuan Zhu⁵®
¹ Department of Astronomy, University of Michigan, West Hall, 1085 South University Avenue, Ann Arbor, MI 48109-1090, USA; earich@umich.edu
² Center for Astrophysics | Harvard & Smithsonian, 60 Garden Street, Cambridge, MA 02138, USA
³ Astrophysics Group, University of Exeter, Stocker Road, Exeter, EX4 4QL, UK
⁴ Physics Department, University of Michigan, Randall Lab, 450 Church Street, Ann Arbor, MI 48109-1090, USA
5 Department of Physics and Astronomy, University of Nevada, Las Vegas, 4505 S. Maryland Parkway, Box 454002, Las Vegas, NV 89154-4002, USA
Received 2021 January 5; revised 2021 April 13; accepted 2021 April 15; published 2021 June 4

Abstract

Dust evolution in protoplanetary disks from small dust grains to pebbles is key to the planet formation process. The gas in protoplanetary disks should influence the vertical distribution of small dust grains (\sim 1 μ m) in the disk. Utilizing archival near-infrared polarized light and millimeter observations, we can measure the scale height and flare parameter β of the small dust grain scattering surface and 12 CO gas emission surface for three protoplanetary disks: IM Lup, HD 163296, and HD 97048 (CU Cha). For two systems, IM Lup and HD 163296, the 12 CO gas and small dust grains at small radii from the star have similar heights, but at larger radii (>100 au), the dust grain scattering surface height is lower than the 12 CO gas emission surface height. In the case of HD 97048, the small dust grain scattering surface has similar heights to the 12 CO gas emission surface at all radii. We ran a protoplanetary disk radiative transfer model of a generic protoplanetary disk with TORUS and showed that there is no difference between the observed scattering surface and 12 CO emission surface. We also performed analytical modeling of the system and found that gas-to-dust ratios larger than 100 could explain the observed difference in IM Lup and HD 163296. This is the first direct comparison of observations of gas and small dust grain height distribution in protoplanetary disks. Future observations of gas emission and near-infrared scattered-light instruments are needed to look for similar trends in other protoplanetary disks.

Unified Astronomy Thesaurus concepts: Protoplanetary disks (1300); Direct imaging (387)

1. Introduction

Protoplanetary disks are composed of dust and gas and host forming and already formed exoplanets. Small dust grains ($\sim 1~\mu m$) and gas interact due to the large amount of drag imparted on small dust grains through gas movement. Thus, the vertical height of small dust grains in the disk should be related to the gas environment of the disk. Thus, if we can independently measure the heights of gas and small dust grains in protoplanetary disks, we can probe fundamental disk characteristics, such as the gas-to-dust ratio and turbulence in the disk.

It is expected that protoplanetary disks where the majority of the mass is in the central star will have a flare shape. This is due to the fact that the internal temperature of the disk decreases more slowly than r^{-1} (Kenyon & Hartmann 1987). The flare shape has subsequently been confirmed through various direct observations of protoplanetary disks (Ginski et al. 2016; Avenhaus et al. 2018; Pinte et al. 2018; Villenave et al. 2020) and theoretically investigated (Meyer & Meyer-Hofmeister 1982; Malbet & Bertout 1991; Bell et al. 1997; D'Alessio et al. 1998; Birnstiel et al. 2010).

The radial height (H(r)) of protoplanetary disks is described by a power law with β as the flare parameter, H_0 as the scale height, and r_0 as the fiducial radius, i.e.,

$$H(r) = H_0 \left(\frac{r}{r_0}\right)^{\beta}.$$
 (1)

We note that in this work, we use $r_0 = 100$ au, and all H_0 values have been adjusted to match this fiducial radius. Theoretical

efforts have taken place to estimate the expected values β . Chiang & Goldreich (1997) showed that for a disk with a surface density profile power law of \sim 1.5 that is irradiated, the maximum flaring parameter value is $\beta = 9/7 \sim 1.3$. Similarly, Kenyon & Hartmann (1987) showed that for a disk with a small disk–to–stellar mass ratio, the expected flaring parameter value should be $\beta = 9/8 = 1.125$ and derive a maximum flare parameter $\beta = 1.25$.

The disk flare parameter β has previously been observationally measured for both gas and dust. Lagage et al. (2006) measured the height of polycyclic aromatic hydrocarbon (PAH) emission for HD 97048, measuring a radial minor axis offset resulting in a scale height H_0 of $34.2^{+0.4}_{-2.2}$ au and $\beta =$ 1.26 ± 0.05 . Additionally, the same technique can be used for multiringed systems for micron-sized particles in near-IR scattered light. Ginski et al. (2016) observed HD 97048 with the Very Large Telescope (VLT) Spectro-Polarimetric Highcontrast Exoplanet REsearch (SPHERE), imaged the scatteredlight rings and gaps in the near-IR, and measured a scale height H_0 of 18.5 au and $\beta = 1.73 \pm 0.05$. Finally, Avenhaus et al. (2018) measured the β flare parameter values in near-IR scattered light for V4046 Sgr (1.605 \pm 0.132), RXJ 1615 (1.116 ± 0.095) , and IM Lup (1.271 ± 0.197) . The same direct and model independent measurements can be performed for ¹²CO gas emission utilizing the spatial and spectral sensitivity of the Atacama Large Millimeter/submillimeter Array (ALMA). Pinte et al. (2018) measured the ¹²CO and ¹³CO gas heights for IM Lup measuring β values of 1.8 ± 0.2 and 2.1 ± 0.4 , respectively. There have been other measurements of

Table 1Gas Disk Parameters

Object	Inc. (deg)	PA (deg)	Spectral Type	Age (Myr)	Distance (pc)	Mass (M_{\odot})	Lum. (L_{\odot})
IM Lup HD 163296 HD 97048	48 ± 3^{a} 42 ± 3^{e} 41 ± 3^{h}	143 ^a 132 ^e 2.8 ⁱ	M0 ^a A1 ^f Be9.5/A0 ^j	1.1 ± 0.2^{b} 6.03^{f} $2-3^{j}$	155.8 ± 0.5 101.0 ± 0.4 184.4 ± 0.8	1° 1.95 ^g 2.5 ^j	0.9 ^d 20.4 ^g 35 ^k

Notes. The listed inclination and disk major axis PA are the assumed values for the CO extraction and are taken from the reference column. The assumed distances for these three targets are from the EDR3 Gaia archive and utilized throughout this work (Gaia Collaboration et al. 2016, 2021). Citations for specific values are given in footnotes.

protoplanetary disk height (e.g., class I source IRAS 04302 +2247; Podio et al. 2020) demonstrating that different molecules and isotopologues probe different heights of the disk. We note that these are all tracers of the gas and dust and are not direct measurements of the gas and dust height in the disk.

While both ¹²CO gas and small grain dust disk heights have been measured, the measurements have never been investigated or compared to test the fundamental properties of the gas vertically supporting small dust grains in protoplanetary disks. In this paper, we will present small dust grain and ¹²CO gas height measurements in Sections 2.1 and 2.2. We will then compare the CO gas and small grain dust height measurements in Section 3. We will then create a typical protoplanetary disk with radiative transfer modeling to test whether the observed surfaces would bias the results (Section 4). We then explore disk parameters that could potentially influence the gas and dust height with a simple analytical disk model in Section 5. Finally, we will discuss how these new findings will affect how we interpret protoplanetary disks and summarize our conclusions in Section 6.

2. Measurements of Gas and Small Dust Grains

There are specific cases in which both the gas height of the disk as a function of radius and the small grain dust height can be measured. First, protoplanetary disks must be moderately inclined ($\sim 30^{\circ}-70^{\circ}$), as height measurement techniques for both take advantage of the three-dimensional inclined disk projected onto the plane of the sky. Second, the CO gas must be plentiful and dense enough to create an optically thick disk photosphere that can be observed. Finally, the protoplanetary disk must host several scattered-light rings in order to measure the small dust grain height as a function of radius. Such measurements probing the gas and dust heights have been made for a host of protoplanetary disks, including HD 163296, IM Lup, HD 97048, and RXJ 1615 (Ginski et al. 2016; Monnier et al. 2017; Avenhaus et al. 2018).

To create our sample, we searched for previously observed protoplanetary systems that had a moderate inclination ($\sim 30^{\circ} - 70^{\circ}$), were young with plenty of CO gas, and were multiringed to enable power-law fits of the small dust grains over multiple

rings. We found that three targets, IM Lup, HD 163296 (MWC 275), and HD 97048 (CU Cha), have previous scattered-light detection with multiple rings and sufficient ALMA observations to resolve the kinematic 12 CO gas disk. Details about each of the three systems can be found in Table 1. Below, we will detail the previous detections and the analysis needed to extract the scale heights (H_0) and flare parameter (β) for our target sample.

2.1. Small Dust Grain Height Measurements

Scattered-light imagery has shown that small dust grains accumulate in rings in protoplanetary disks. If we assume that those rings are circular, we can fit ellipses to the peak flux and then calculate the radius of the ring (major axis) along with a minor axis offset due to the height of the dust grains projected onto the plane of the sky. We will utilize previous literature measurements from Avenhaus et al. (2018; IM Lup), Ginski et al. (2016; HD 97048), and Monnier et al. (2017) and Rich et al. (2020; HD 163296). The radii and measured heights of these rings can be found in Table 2, and the values are plotted in green in Figure 1. We note that we reinterpret one of the second ring height measurements made by Ginski et al. (2016), which can be found in the Appendix. With the exception of the second ring around HD 163296, all of the other rings were imaged in polarimetry mode from the Gemini Planet Imager (GPI) or SPHERE. The second ring listed from HD 163296 was taken in the coronographic mode of the Hubble Space Telescope's Space Telescope Imager and Spectrograph (STIS) instrument. These observations are total intensity images and do not have any polarization information. We assume that the most common origin of the total intensity light from this second ring is from scattered light from the top of the disk and interpret the observations as we did for the other near-IR scattered-light observations. Additionally, STIS in coronographic mode is filterless; thus, light from optical blue to near-IR was included in the image. The second ring in HD 163296 might be sensitive to smaller dust grains and at a different dustscattering height than the other rings imaged with either GPI or SPHERE in the near-IR.

Objects HD 97048 and HD 163296 have further known rings that are not discussed in this work. In the case of HD 97048,

a Cleeves et al. (2016).

^b Avenhaus et al. (2018).

^c Panić et al. (2009).

^d Hughes et al. (1994).

^e Isella et al. (2016).

f Manoj et al. (2006).

^g Wichittanakom et al. (2020).

h Walsh et al. (2016).

i Ginski et al. (2016).

^j van den Ancker & de Winter (1998).

k Vioque et al. (2018).

Table 2
Small Grain Ring Heights

Object	Ring	Radius (au)	Height (au)	Band	Reference
IM Lup	Ring 1	91.9 ± 3.17	16.5 ± 2.75	H band	Avenhaus et al. (2018)
IM Lup	Ring 2	152.11 ± 4.75	27.4 ± 6.1	H band	Avenhaus et al. (2018)
IM Lup	Ring 3	240.84 ± 4.75	55.4 ± 9.6	H band	Avenhaus et al. (2018)
IM Lup	Ring 4	332.75 ± 12.68	83.2 ± 16.6	H band	Avenhaus et al. (2018)
HD 163296	Ring 1	66.4 ± 3.0	18.0 ± 2.0	J band	Monnier et al. (2017)
HD 163296	Ring 2	328 ± 10.0	64.0 ± 10.0	Clear filter	Rich et al. (2020)
HD 97048	Ring 1	54.4 ± 0.7	1.9 ± 1.9	J band	Ginski et al. (2016)
HD 97048	Ring 2	172 ± 4	32.3 ± 1.5	J band	Appendix

Note. This table lists the ring heights and midplane radial distances of each of the objects. The assumed distances to each target are from Gaia EDR3 and can be found in Table 1.

there are two rings at a further radial extent than those listed in Table 2 (Ginski et al. 2016). However, these two external rings have only been observed with total intensity imaging using angular differential imaging reduction techniques that are known to alter the shape of continuous objects; thus, we did not include these rings in our analysis. For HD 163296, there are two rings between the 77 and 360 au rings listed in Table 2, but these have only been seen with ALMA in either millimeter dust grains or CO gas and never at optical or near-IR wavelengths (Rich et al. 2020).

We fit power laws for each of the objects following Equation (1), where the values of the β flare parameter and scale height (H_0) are in Table 3 and plotted as the green dashed lines in Figure 1. We used python's curve fit package to fit the points and performed a Monte Carlo of the point height uncertainties to estimate the uncertainty of β and scale height (H_0). We explored parameter space values of zero to 4 for β and zero to 200 au for H_0 . We note that the distributions of values for β and H_0 are not symmetric around the median value; thus, for the small dust grain results, we have utilized asymmetric error bars as shown in Table 3. For the HD 97048 result, the first ring has an error bar consistent with zero height from the midplane. This has resulted in β values that can be unphysically large, and the values presented should be considered lower limits for the potential β flare parameter values for small dust grains in HD 97048.

2.2. CO Gas Height Measurements

Data for the ¹²CO gas measurements are from previous works or utilize the ALMA archive reductions. Observations of HD 163296 and IM Lup were taken as part of the Disk Substructure at High Angular Resolution (DSHARP) program (Program ID 2016.1.00484.L; Andrews et al. 2018).⁶ The DSHARP archive provides calibrated ¹²CO data cubes. See Andrews et al. (2018) for a full description of the data reduction description. The HD 97048 data were taken from the ALMA archive (Program ID 2016.1.00826.S) reduced using the ALMA automatic reduction pipeline that produced the ¹²CO data cube

To measure the height of the CO gas disk, we utilize the techniques first described in Pinte et al. (2018) and use the python package by Teague (2019). In summary, the program rotates the CO disk cube such that the disk major axis position angle (PA) in the data cube is horizontal and the closest side of the disk to Earth is at the top of the image. Pixels in the data

cube with low signal-to-noise ratios are masked prior to finding the maximum flux values. Vertical pixel slices are taken along the disk in every frame in the cube to find local maxima corresponding to the 12 CO emission. The brightest flux pixel of each column is taken to be the front side of the disk, and the second-brightest flux pixel is the bottom of the disk. Using the pixel locations of the front (x, y_f) and back (x, y_b) sides of the disk, with the prior knowledge of the disk's inclination (i) and the star's location (x_s, y_s) , the midplane radius r is given by

$$r = \sqrt{(x - x_s)^2 + \left(\frac{y_f - y_c}{\cos(i)}\right)^2}$$
, (2)

and height h has the form

$$h = \frac{y_c - y_s}{\sin(i)}. (3)$$

The y-coordinate center (y_c) is the average of the y_f and y_b values

The python package outputs a set of radii (r), heights (h), and flux values for the disk. We further refined the set of points by removing any heights that had negative values and radii that were beyond 4''. We binned the data in midplane radius with bin sizes of 10 au and applied a median clip to remove further extraneous points. The binned median values along with error bars estimated via median absolute deviation (MAD) and the inclination uncertainty added in quadrature are shown in Figure 1.

We fit the power law in log-log space with the best-fit values shown in Table 3 and plotted in Figure 1. The fits were done on the individual radial and height points, and the linear regression fits were bootstrapped to estimate the errors. All three targets have a broken power-law distribution; thus, we only fit between 50 and 250 au.

3. Comparison of CO Gas and Small Dust Grains

We were able to measure the ^{12}CO gas flare parameter β for IM Lup (1.77 \pm 0.04), HD 163296 (1.39 \pm 0.04), and HD 97048 (1.81 \pm 0.14). Our IM Lup β measurement is well matched to the previous measurement of 1.8 \pm 0.2 (Pinte et al. 2018) and is the only CO gas flare parameter β that had previously been measured. Both IM Lup and HD 97048 have β parameter values that are much larger than the estimated maximum theoretical values (1.3, Chiang & Goldreich 1997; 1.25, Kenyon & Hartmann 1987). However, the β parameter of HD 163296 is more consistent with the theoretical maximum

⁶ https://almascience.eso.org/almadata/lp/DSHARP/

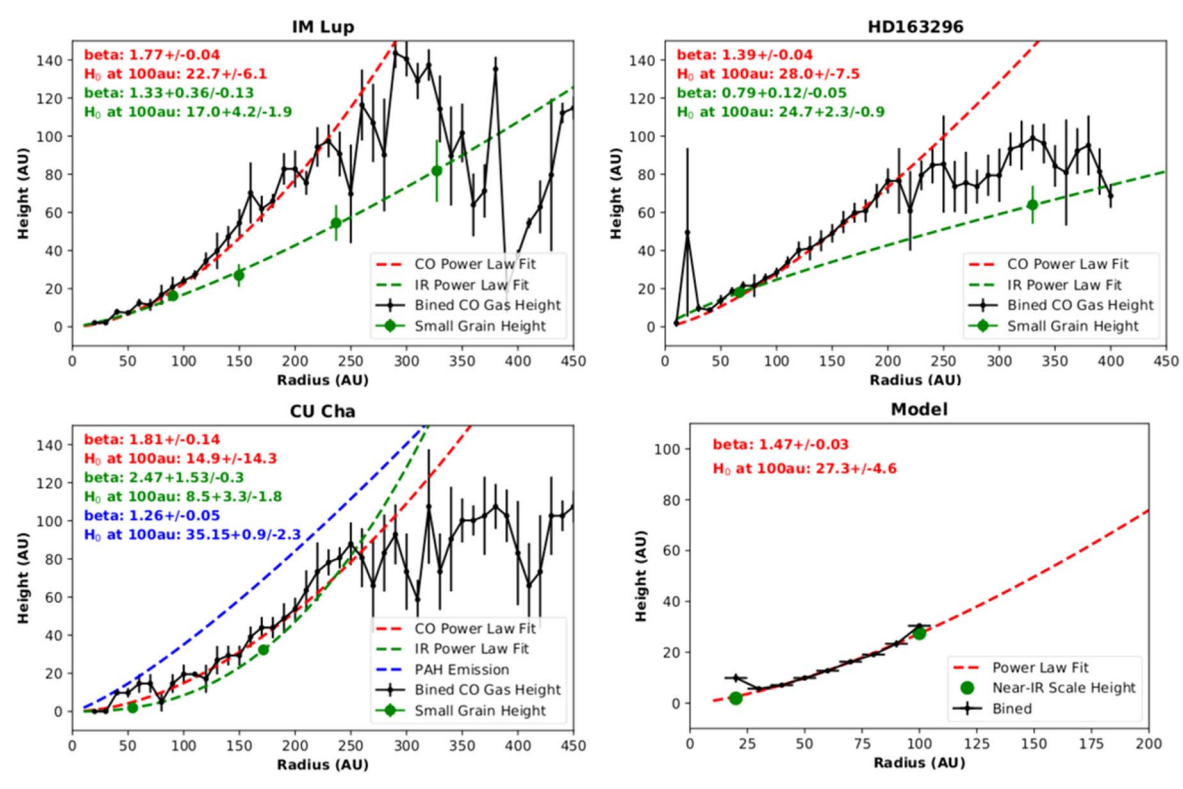


Figure 1. Measured heights of dust and gas as a function of radius for objects IM Lup (upper left), HD 163296 (upper right), HD 97048 (lower left), and a model protoplanetary disk (lower right). Measurements of the ¹²CO disk photosphere are shown in black, small dust grain heights are shown in green, and measured PAH emission is shown in blue, published by Lagage et al. (2006). Power-law fit values are shown in the upper left corner of each panel, and the colors correspond to the colors of the lines.

Table 3
Gas and Small Grain Power-law Fit Results

Object	¹² CO β	$^{12}CO\ H_0\ (au)$ at $r = 100\ au$	Dust β	Dust H_0 (au) at $r = 100$ au
IM Lup	1.77 ± 0.04	22.7 ± 6.1	$1.34^{+0.35}_{-0.13}$	17.0+4.1
HD 163296	1.39 ± 0.04	28.0 ± 7.5	$0.79^{+0.12}_{-0.05}$	$24.7^{+2.3}_{-0.9}$
HD 97048	1.81 ± 0.14	14.9 ± 14.3	$2.48^{+1.52}_{-0.3}$	$8.5^{+3.3}_{-1.8}$

Note. Measured β flare parameter and H_0 scale height for small dust grains and ¹²CO plotted in Figure 1. Parameters H_0 and β are defined in Equation (1).

values. This could be an indication of age, as HD 163296 is estimated to be older than IM Lup and HD 97048 (see Table 1).

We were also able to measure the small grain dust β flare parameter for IM Lup $(1.34^{+0.35}_{-0.13})$, HD 163296 $(0.79^{+0.12}_{-0.05})$, and HD 97048 $(2.48^{+1.52}_{-0.3})$. Both IM Lup and HD 163296 have β flare parameter values that are broadly consistent with a maximum theoretical β value (1.3, Chiang & Goldreich 1997; 1.25, Kenyon & Hartmann 1987), while HD 97048's measured β is much larger. This was previously noted by Avenhaus et al. (2018) and Pinte et al. (2018). We do not have a good constraint on the β parameter value for HD 163296 and HD 97048, as there are only two points. Our measured values for IM Lup are consistent with the values measured by Avenhaus et al. (2018; 1.271 \pm 0.197), while our HD 97048 measurement is much larger than that of Ginski et al. (2016; 1.73 ± 0.05). However, Ginski et al. (2016) utilized height measurements for all four rings and the heights of the gaps, and we have recalculated the estimated height for the second ring in HD 97048 in the Appendix. Thus, our estimate is more

conservative, as we avoid angular differential imaging (ADI) total intensity artifacts as discussed above and the assumption of a large wall at ring 2 in the HD 97048 system.

Here we caution against direct comparisons between the observed emission and scattering surface of the ^{12}CO gas and small dust grain surfaces to theoretical values of the gas and dust heights, as previously noted by Avenhaus et al. (2018) and Pinte et al. (2018). As noted in Section 1, the measured flaring parameter β does not represent the physical height of the disk but the observed height of the disk that is dependent on the temperature of the disk (for CO) and the dust-scattering properties (for small dust grains). We will begin to address this issue in Section 4.

Finally, we compare the height as a function of radius of CO gas and the small dust grains. Notably, in all three systems, the first ring is colocated with the ¹²CO gas emission layer, as shown in Figure 1. For systems IM Lup and HD 163296, the scattered-light rings have smaller heights than the ¹²CO gas emission layer. This is confirmed, as the 12 CO gas has a β flare parameter value of 1.77 ± 0.04 that is 1σ larger than the small dust grains β of 1.34 $^{0.35}_{-0.13}$. Though there are fewer rings, HD 163296 seems to show the same trend as IM Lup. However, this same trend is not seen in the case of HD 97048, where both of the rings appear to be colocated with the CO gas, and the β flare parameter is larger rather than smaller. Thus, in the case of some protoplanetary disks, it appears that there is a radial dependence of a disk when comparing the ¹²CO gas emission height and the small dust grain height. We note that the second ring in HD 163296 and the fourth ring in IM Lup are located exterior to the ¹²CO power-law break.

Table 4
Model Parameters

Parameter	Value
$T_{\rm eff}$ (K)	9250
$M_{ m star}~(M_{\odot})$	2.5
$M_{ m disk} \; (M_{\odot})$	0.2
Disk density exponent (α_{den})	2.0
Disk scale height exponent (β)	1.4
Disk scale height (H_0 ; au)	10
Small dust grain size range (μ m)	0.7-2
Large dust grain size range (mm)	0.9-1

Note. Subset of TORUS parameters for the simple protoplanetary disk model. The $^{12}\mathrm{CO}$ emission surface and small dust grain scattering surface measurements are shown in Figure 1. Note that the disk density exponent α is different from the α turbulent viscosity coefficient discussed in Section 5.

4. Simple Protoplanetary Disk Model

An issue remains in that we are not tracing the true gas or dust scale height of the disk. In the case of the ^{12}CO gas, the emission comes from the photosphere of the disk, which is dependent on the local temperature of the disk and the ^{12}CO abundance. For the small dust grains, the height is tracing the local illumination from the protostar onto the disk and the scattering efficiency of the dust grains. In both cases, and especially the scattering efficiency of the small dust grains, to calculate the true gas or dust scale height from the observables is difficult due to degeneracies and unknown quantities of the disk material. We choose to approach this problem by performing radiative transfer modeling of a generic two-ringed protoplanetary disk and see if a model 12 CO ALMA image and an H-band scattered-light image show any relative difference.

We model our simple protoplanetary disk using the radiative transfer program TORUS (Harries 2000; Harries et al. 2004; Rundle et al. 2010; Harries 2011). TORUS is a Monte Carlo radiative transfer code using an adaptive mesh and radiative equilibrium method described in Lucy (1999). We utilized atomic and molecular lines from the LAMDA database (Schöier et al. 2005) and CO energy level coefficients from Müller et al. (2005). We parameterized a generic protoplanetary disk in 2D to be composed of CO gas, small dust grains $(0.7-2 \mu m)$, and large dust grains (0.9-1 mm) using a grain prescription from Draine & Lee (1984). Stellar and disk parameters are based on Rich et al. (2019), who modeled the protoplanetary disk system HD 163296. The disk has a disk density exponent α of 2.0 and a disk scale height exponent β of 1.4 for the dust and gas. The dust grains are defined as a fraction of the gas height, with the small dust grains having 70% of the gas scale height and the large dust grains having 10% of the gas scale height. We modeled two rings at 25 and 100 au from the star with ring widths of 1 au. We included CO freeze-out for $T < 30 \,\mathrm{K}$ and CO dissociation using quenching rates from Yang et al. (2010). This should accurately replicate the ¹²CO disk emission surface observed by ALMA. A subset of model parameters is shown in Table 4.

Using the model parameters described above, TORUS produced a scattered-light *H*-band image of the two scattered-light rings and a ¹²CO data cube. The two model data sets were convolved to match SPHERE/IRDIS and ALMA resolution, respectively. We processed the model ¹²CO data cubes using the same process described in Section 2.2. Similarly, we fit ellipses to the rings as described in the Appendix. The results

are plotted in Figure 1, where the green points are the small grain heights, the black points are the CO gas height, and the red dotted line is the best-fit power law. As shown in Figure 1, both of the scattered-light rings are colocated with the $^{12}\mathrm{CO}$ gas emission. The measured flare parameter β is 1.47 ± 0.03 , very similar to the input disk scale height exponent of 1.4. Thus, we can see the effect that the flare shape of the $^{12}\mathrm{CO}$ gas is not necessarily the same as the true CO gas flare shape. Finally, our simple model demonstrates that our observable tracers of the dust and gas height, $^{12}\mathrm{CO}$ emission surface, and small dust grain scattering surface have similar flare profiles.

5. Analytical Disk Model

We next want to explore the disk parameters that could cause the difference in β flare parameter values between the small dust grain scattering surface and ^{12}CO gas emission. We choose to use a parametric structure model of an exponentially tampered accretion disk profile in hydrostatic equilibrium and the parameterizations and equations outlined in Williams & Best (2014). In summary, we define the pressure scale height, H_P , as

$$H_P = \frac{kT_{\text{mid}}r^3}{\text{GM}_{\text{star}}\mu m_H},\tag{4}$$

where r is the midplane radius of the disk, $T_{\rm mid}$ is the midplane temperature of the disk at r, $M_{\rm star}$ is the mass of the protostar, and μ is the mean molecular weight of the gas. The midplane temperature is defined as a power law as

$$T_{\text{mid}}(r) = T_{\text{mid},1} \left(\frac{r}{1 \text{ au}}\right)^{-q},\tag{5}$$

where we assume values of $T_{\text{mid},1} = 200 \text{ K}$ and q = 0.55 as assumed in Williams & Best (2014).

The temperature structure of the disk utilized in Williams & Best (2014) defines the ^{12}CO emission region. For temperatures T < 20 K, the CO will freeze out, creating the lower boundary region, and the upper boundary is defined by CO dissociation when the column density of H_2 reaches $1.3 \times 10^{21} \text{ H}_2 \text{ cm}^{-2}$. Since the ^{12}CO emission layer is optically thick, the location of the ^{12}CO emission will be slightly below the upper boundary; thus, we only plot the upper ^{12}CO emission as a tracer for the ^{12}CO emission. The ^{12}CO upper emission layers are shown in Figure 2 as dashed lines.

Next, we can calculate the small dust grain pressure height using the gas pressure height. We follow the parameterization of the dust pressure height (H_d) as outlined in Pohl et al. (2017) as

$$H_d(r, a) = H_p(r) \times \min\left(1, \sqrt{\frac{\alpha}{\min(St, 1/2)(1 + St^2)}}\right). \quad (6)$$

We define α as the viscosity parameter, a as the dust grain diameter, r as the midplane radius, and St as the Stokes number, where $St = \rho a\pi/\Sigma_g 2$. We utilize the same gas surface density power law with an exponential taper (Σ_g) as defined in Williams & Best (2014) and assume a dust grain volume density of 1.2 g cm⁻³ as used in Pohl et al. (2017).

Having obtained the dust pressure height (H_d) , we now estimate where the dust-scattering layer is located. Using the dust opacities, we calculated the line of sight from the star to that radial bin in the disk and found the height at which the

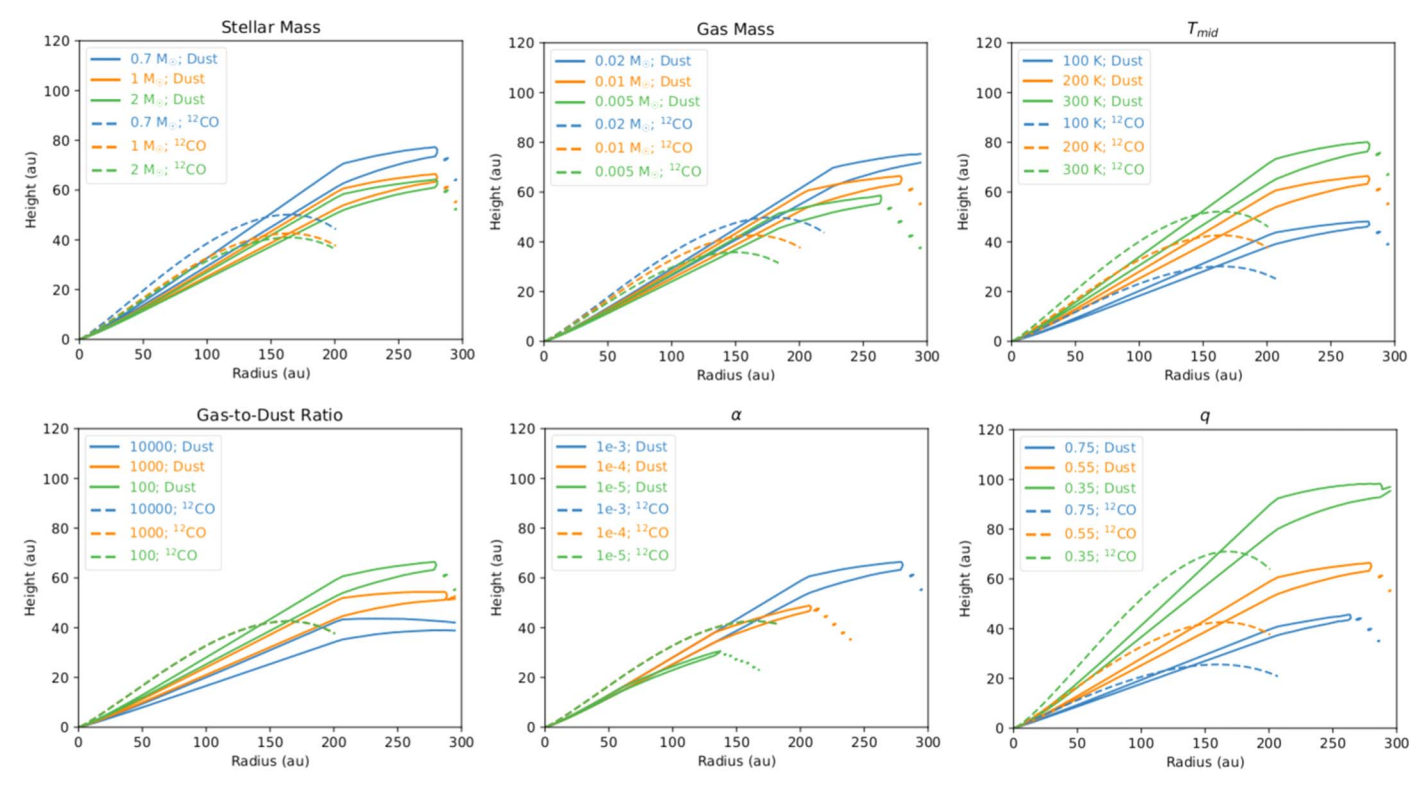


Figure 2. Results of analytical modeling varying the solar mass (top left), disk gas mass (top middle), $T_{\rm mid}$ (top right), gas-to-dust ratio (bottom left), α (bottom middle), and midplane temperature exponent q (bottom right) parameters. The dashed lines show the upper region of the CO-emitting photosphere of the disk, and the solid lines show the scattering surface containing 80% of the scattering flux. The base models are defined by the parameters: $\gamma = 0.75$, $\psi = 0.2$, $R_c = 60$ au, $R_{\rm in} = 1.0$ au, $M_{\rm gas} = 0.01~M_{\odot}$, $M_{\rm star} = 1~M_{\odot}$, $T_{\rm mid} = 200~{\rm K}$, $T_{\rm atm} = 1000~{\rm K}$, $\alpha = 10^{-3}$, q = 0.55, and a = 1e-5.

largest number of scattering events would occur. We plotted contours that are 80% of the maximum scattering events that occur, as shown in Figure 2 (solid lines). Thus, the values plotted in Figure 2 are parametric models of the observed quantities plotted in Figure 1.

We explore the effect that six parameters $(M_{\text{star}}, M_{\text{gas}}, T_{\text{mid}})$ gas-to-dust ratio, viscosity parameter α , and q) have on the difference between the ¹²CO emission and the small dust grain scattering surface. The first parameter, $M_{\rm star}$, has a direct effect on the pressure scale height of the gas, as shown in Equation (4). We note that with a changing stellar mass, we also expect a change in stellar luminosity (L) and thus a change in the midplane temperature of the disk (T_{mid}) , which will affect the disk height structure as well. In order to account for this, we utilize Equation (12c) in Chiang & Goldreich (1997), where the internal disk temperature $T_{\rm mid} \propto T_{\rm eff} \times R_*^{1/2}$. Thus, the luminosity of the star $L \propto T_{\rm mid}^4$. As seen in Equation (4), the $T_{\rm mid}$ and $M_{\rm star}$ terms are proportional; thus, any change in $M_{\rm star}$ could be canceled out by an equal change in T_{mid} . However, the mass and luminosity relationship for protostars is complicated; thus, we assumed masses and luminosities for two of our objects, IM Lup (0.7 M_{\odot} , 1.56 L_{\odot}) and HD 163296 (1.95 M_{\odot} , 20.4 L_{\odot} ; Avenhaus et al. 2018; Wichittanakom et al. 2020). We scaled the $T_{\rm mid}$ value from the luminosity assuming a luminosity of 1.56, 1.75, and 20.4 for each of the corresponding solar-mass values of 0.7, 1.0, and 2 M_{\odot} . As seen in Figure 2, the ¹²CO emission height and small dust grain scattering surface are equally affected by the change of stellar mass and luminosity.

Next, we varied the total gas mass $M_{\rm gas}$ of the system, which changes the surface density of the gas. As shown in the top

middle panel in Figure 2, this parameter equally affects both the ^{12}CO gas emission height and small dust grain scattering surface height. Thus, the total gas mass M_{gas} cannot explain the difference in the observed gas and dust heights in these disks.

We explored the global gas-to-dust ratio in the disk. We assumed nominal values of G/D = 100 and explored parameter values by factors of 10 to see if these values could explain the gas and dust height differences. As shown in Figure 2, changing the gas-to-dust ratio has no effect on the observed ¹²CO gas height (dashed lines are plotted on top of each other) but does affect the small dust grain scattering surface heights. By varying the gas-to-dust ratio, we are effectively lowering the amount of dust in the system and thus lowering the height of the scattering layer of the disk. This appears to replicate what we observe in the IM Lup and HD 163296 systems, as shown in Figure 1. We note that we are assuming in our simplified models that the gas-to-dust ratio is constant throughout the disk. This is unlikely to be true in terms of height from the midplane due to dust settling. More sophisticated modeling is needed with a nonconstant gas-todust ratio to show that the similar trend is true.

We explored the effects that the assumed disk temperature structure might have on the radial height of ^{12}CO and small dust grains by varying the midplane temperature, T_{mid} , and midplane temperature exponent, q, as defined in Equation 5. We note that changing T_{mid} is similar to changing the luminosity of the star as discussed above when varying the stellar mass parameter. When decreasing values of T_{mid} , the slope of both the ^{12}CO and small dust grain surfaces decreases, with the slope of the ^{12}CO surface decreasing faster. However, this is unlikely to explain the surface height differences, as IM Lup and CU Cha have similar β values but different resulting

surface heights for small dust grains and ^{12}CO gas. Next, we varied q where increasing the value of q decreased the slopes of ^{12}CO and small dust grain surfaces. Similarly to T_{mid} , the ^{12}CO surface slope decreased faster than the small dust grain slope. However, in a similar argument for T_{mid} , this would not explain the difference between IM Lup and CU Cha.

The last parameter explored was the α turbulent viscosity coefficient shown in Figure 2. Note that the turbulent viscosity coefficient is usually denoted as α in the literature, which is not to be confused with the disk density exponent α used in Section 4. We assumed a nominal value of $\alpha = 10^{-3}$ and explored factors of 10 smaller. Similar to the gas-to-dust ratio, the α viscosity parameter does not effect the ¹²CO gas emission height. By decreasing the value of the α viscosity coefficient, the scattering surface for small dust grains is lower. The α viscosity parameter could potentially explain the scale height deviation we observe for HD 163296 and IM Lup, as shown in Figure 1. However, the amount of turbulence in IM Lup and HD 163296 has been measured, roughly translating to $\alpha = 1 \times 10^{-3}$ (Hughes et al. 2011; Flaherty et al. 2017). A lower value of α is needed to explain the height disparity in small grains versus ¹²CO gas by a factor of ×10–100, making this explanation unlikely.

6. Discussion and Conclusions

We have measured the flaring parameter β for the ¹²CO gas emission surface of protoplanetary disks around IM Lup, HD 163296, and HD 97048 and compared it to previous measurements of small dust grain scattering surface heights. We find that for IM Lup and HD 163296, small dust grain heights are colocated with the CO gas emission at small radii from the star but not at radii larger than >100 au. However, for HD 97048, we find that the small dust grain heights and CO gas emission are colocated throughout the disk. With simple radiative transfer modeling of a protoplanetary disk, we were able to show the expectation that the small dust grain scattering surface is at a similar height to the ¹²CO gas emission layer.

Though we cannot definitively determine any trends with a sample size of three disks, we can look for potential trends for future investigations. While the disks around IM Lup and HD 163296 show the same radial trend, the two systems have little in common, as HD 163296 (7.6 Myr) is much older than IM Lup (1.1 Myr); IM Lup is a T Tauri M0 star, while HD 163296 is a Herbig Ae A1; and IM Lup is a solar-mass star (1 M_{\odot}), and HD 163296 is twice as massive (1.95 M_{\odot}). In fact, HD 163296 has the most in common with HD 97048, as they are both Herbig stars and more massive, with HD 97048 being the most massive star at 2.5 M_{\odot} . It appears that vertical heights of gas and dust trends may not simply be a function of mass, age, or spectral type. Increasing the number of protoplanetary disks in which we have measured gas and small dust grain heights is necessary to fully investigate disk parameter trends such as age, mass, and stellar host star.

There are several caveats when comparing our sample of three targets to a generic protoplanetary disk. First, the mechanism(s) for formation of the dust rings themselves are unknown (e.g., protoplanets, ice lines), and these mechanisms and environments could potentially influence the vertical distribution of the small dust grains within these rings. For example, illumination from the star or an accreting protoplanet can increase the vertical height of the disk, similar to what occurs

in the inner disk (Dullemond et al. 2001; Natta et al. 2001; Montesinos et al. 2021). If these mechanisms play an important role in the vertical distribution of small dust grains, what we are observing may not be ubiquitous for all protoplanetary disks but only for protoplanetary disks that have rings caused by the mechanism at hand. Modeling of the various mechanisms that cause ring formation in protoplanetary disks and the influence of the vertical gas and dust structure is needed. Second, we assume that these rings are circular and centered around the central star. However, there is evidence that some systems (e.g., HD 169142, Bertrang et al. 2018; GW Ori, Kraus et al. 2020) have offset rings; thus, this assumption is defiantly not valid for all protoplanetary disk systems. Alternative measurements of small dust grain heights that are not dependent on the presence of rings in protoplanetary disks while also dealing with the intricacies of interpreting scattered-light images are needed to avoid the dust ring issues. Finally, different isotopologues of CO and different molecules will trace lower layers in the disk that might correlate differently with the small dust grain heights than ¹²CO. Future work is needed to investigate the correlation of other molecule emission heights in the disk to small dust grain scattering surface heights.

One issue of our sample is that these systems have much larger disks than a typical protoplanetary disk of around 100 au. What we could be observing is that beyond 100 au, the disks are not behaving like our archetypal model as described in our analytical model (Section 5). Future investigations of more typically sized protoplanetary disks are necessary to verify if the observed dust and gas height deviation is present in smaller disks as well. In line with this caveat, we also assume that our disks have a continuous power law with no breaks at all. However, power-law breaks have previously been identified in protoplanetary disk systems for both scattered light and ¹²CO gas (Wisniewski et al. 2008; Pinte et al. 2018; Teague et al. 2018). This aspect is important, as two scattered-light rings, in HD 163296 and IM Lup, are exterior to the ¹²CO gas powerlaw break. Additionally, the optical depth of the ¹²CO gas could play an important part in the outer disk, as the gas becomes optically thin. While we are unable to investigate this caveat due to the limited number of rings in our systems, future work needs to investigate the effect of scale height with broken power-law height systems.

We investigated six stellar and disk parameters ($M_{\rm star}$, $M_{\rm gas}$, $T_{\rm mid}$, gas-to-dust ratio, α , and q) that might explain the flared discrepancy of gas and dust as seen in IM Lup and HD 163296. The stellar mass, total gas mass, T_{mid} , and q parameters are unlikely to explain the discrepant flare trend. Both the gas-todust ratio and viscosity parameter α could potentially explain the β flare parameter in IM Lup and HD 163296. However, the α viscosity parameter would have to be unusually small and requires further investigation. If the gas-to-dust ratio is largely responsible for explaining the discrepancy between the difference in β flare parameters for small dust grains and gas, our height comparison methods might be good tracers of the gas-to-dust ratios in the top layers of protoplanetary disks. We note that this treatment of disk temperature is very simplistic, and future research on its effect on the height of small dust grains and ¹²CO gas is needed.

Another potential mechanism to explain the radial dependence of the CO gas and small dust grain height deviation is dust settling. Modeling by Facchini et al. (2017) shows that lower turbulence in the disk can result in the same type of radial

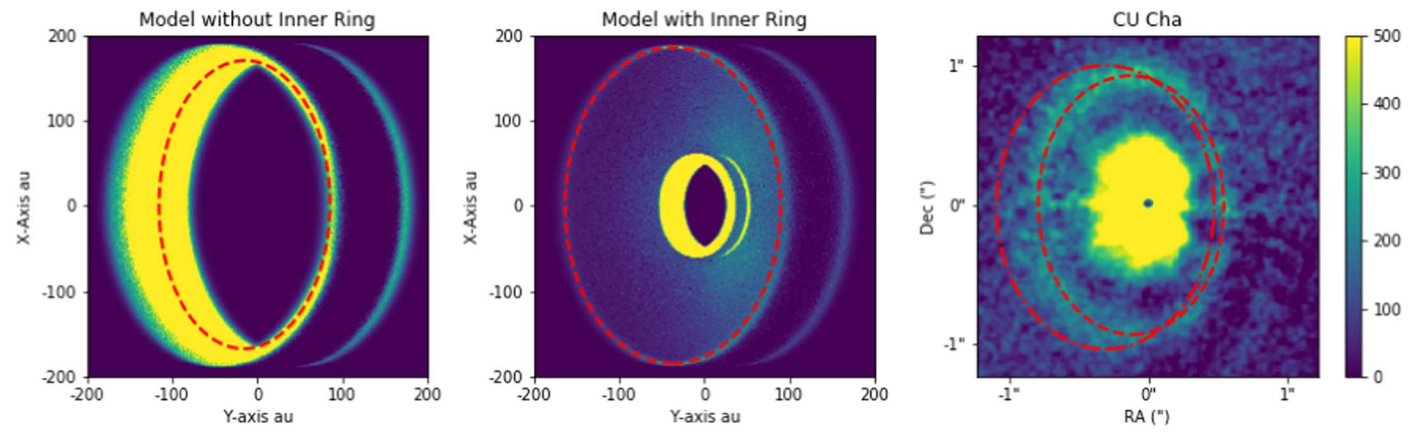


Figure 3. Polarized light TORUS models (left and center) demonstrate that the second ring in the protoplanetary disk HD 97048 (right) is unlikely to have a large wall. The left panel is a TORUS model with a dusty ring located at 188 au, and the dashed red line shows the best ellipse fit of the disk. The middle panel is a TORUS model with two dusty rings located at 55 and 188 au, and the red dashed line is the best-fit ellipse for the outer ring. The right panel shows the scattered-light *J*-band image of HD 97048, with the red dashed line as our best-fit ellipse to the observed data and the dotted–dashed line as the best-fit ellipse from Ginski et al. (2016).

dependence we observe, where the small dust grains appear to decouple in height from the CO gas as one travels outward radially. Thus, by measuring the CO gas and small dust grains, we could potentially constrain the turbulence in the disk. This aligns with our analytical model discussed in Section 5. However, there have been turbulence measurements of HD 163296 that are consistent with a viscosity parameter value of $\alpha = 1 \times 10^{-3}$ (Hughes et al. 2011; Flaherty et al. 2017). According to our analytical model in Section 5, this amount of viscosity in the disk may not be enough to explain the CO gas and small dust grain heights. Thus, lower turbulence in the disk is unlikely to have caused the radial dependence of the CO gas and small dust grain height deviation for HD 163296. More observationally direct measurements of the protoplanetary disk turbulence are needed to see if HD 163296 turbulence measurement is an outlier when compared to turbulence measurement of other disks such as HD 97048 and IM Lup. Future hydrodynamical modeling work is needed that includes an exploration of the turbulence in the disk that also outputs gas and dust scale height observables such as the ¹²CO emission surface and the small dust grain scattering surface.

Thanks to Dr. Henning Avenhaus and Dr. Christian Ginski for supplying SPHERE/IRDIS images for IM Lup and HD 97048, respectively. E.A.R. acknowledges support from NSF AST 1830728. This work has made use of data from the European Space Agency (ESA) mission Gaia (https://www.cosmos.esa.int/gaia), processed by the Gaia Data Processing and Analysis Consortium (DPAC; https://www.cosmos.esa.int/web/gaia/dpac/consortium). Funding for the DPAC has been provided by national institutions, in particular the institutions participating in the Gaia Multilateral Agreement.

Appendix Reinterpreting the Rings around HD 97048

Previous near-IR observations with VLT/SPHERE of the protoplanetary disk HD 97048 (CU Cha) by Ginski et al. (2016) found four dusty rings at 46, 161, 272, and 341 au. Ginski et al. (2016) fit ellipses to the rings, where the first two inner ring fits (46 and 161 au) were to scattered-light imaging and the two outer ring fits (272 and 341 au) were to total intensity imaging with an angular differential imaging technique reduction. For all four rings, Ginski et al. (2016)

measured a minor axis offset associated with a projected scale height of the disk. They noted that the second ring might possibly be biased by hosting a partially illuminated "wall" that would influence the measured height on the far side of the disk (left side). Thus, the flux observed is not only from the top of the ring but closer to the midplane of the disk. This can bias the ellipse fitting of the ring, as the wall will be fully illuminated from the view of the observer, making the minor axis of the ring appear to be smaller than in reality (see left panel of Figure 3). To avoid the ring location being biased by the wall, Ginski et al. (2016) only fit an ellipse to the forward part of the disk, avoiding areas where a potential wall is fully illuminated. The explanation of a wall being present at the second ring is unexpected, as walls are typically associated with the inner disk, and in the case of HD 97048, there is scattered-light flux traced to the inner working angle of the VLT/SPHERE images. We would expect that the inner small dust grain material would shadow the second ring and not allow for the wall to be illuminated.

To test whether one expects to be strongly biased by a wall in HD 97048 with the presence of inner disk material, we performed a simple scattered-light radiative transfer modeling using the TORUS of a single-ringed system and a two-ringed disk shown in Figure 3. We utilized the same TORUS model parameters as described in Section 4, with the exception that the two rings are located at 46 and 188 au. The left panel in Figure 3 shows a single ring located at 188 au from the star and is fully illuminated, creating a wall. The dashed red line shows the best-fit ellipse, which is strongly biased by the presence of a wall and does not trace the top of the disk. This single-ringed scenario is the bias that Ginski et al. (2016) sought to avoid by only fitting an ellipse to the right side of the disk. However, the full wall is not expected to be illuminated, as the presence of the inner ring at 46 au will shadow the wall. The middle panel in Figure 3 shows a two-ringed disk system where the interior ring shadows the outer ring. When we now fit the ellipse to the outer ring in our model, we find that the ellipse traces the true height of the disk. Thus, we do not expect to see the effect of a wall in the HD 97048 system.

We fit an ellipse to the second ring of the HD 97048 VLT/SPHERE H-band data. We found the full ellipse of the second ring and a minor axis offset of 0.1259 ± 0.013 , which, assuming an inclination of 44° , results in a scale height of

Table 5
Gas Disk Parameters

Parameter	Ring 2
Radius (au)	172 ± 4
Inclination (deg)	44 ± 3
Major axis offset (arcsec)	0.002 ± 0.018
Minor axis offset (arcsec)	0.1259 ± 0.0013
Disk height (au)	32.3 ± 1.5

 32 ± 1.5 au at a projected radius of 172 ± 4 au. Our ellipse measurements for the second ring can be found in Table 5 and are shown in Figure 3. The presence of a wall can strongly bias the inclination measurement by affecting the ratio of the major to minor axis. Our measured inclination of $44^{\circ}\pm3^{\circ}$ is consistent with the PAH emission isophot fitting (Lagage et al. 2006) and ALMA disk inclination fitting of 41 ± 3 (Walsh et al. 2016). We note that the inclination of 39.9 ± 1.8 is also consistent with those two alternative measurements. We cannot exclude a wall being present in the HD 97048 data. However, there is no evidence to suggest that the added complexity to the ringed structure is needed. Thus, for this work, we utilize our ellipse fit measurement of the second ring in the HD 97048 system.

ORCID iDs

Evan A. Rich https://orcid.org/0000-0002-1779-8181
Richard Teague https://orcid.org/0000-0003-1534-5186
John D. Monnier https://orcid.org/0000-0002-3380-3307
Claire L. Davies https://orcid.org/0000-0001-9764-2357
Arthur Bosman https://orcid.org/0000-0003-4001-3589
Tim J. Harries https://orcid.org/0000-0001-8228-9503
Nuria Calvet https://orcid.org/0000-0002-3950-5386
Fred C. Adams https://orcid.org/0000-0002-8167-1767
David Wilner https://orcid.org/0000-0003-1526-7587
Zhaohuan Zhu https://orcid.org/0000-0003-3616-6822

References

Andrews, S. M., Huang, J., Pérez, L. M., et al. 2018, ApJL, 869, L41
Avenhaus, H., Quanz, S. P., Garufi, A., et al. 2018, ApJ, 863, 44
Bell, K. R., Cassen, P. M., Klahr, H. H., & Henning, T. 1997, ApJ, 486, 372
Bertrang, G. H. M., Avenhaus, H., Casassus, S., et al. 2018, MNRAS, 474, 5105

Birnstiel, T., Dullemond, C. P., & Brauer, F. 2010, A&A, 513, A79 Chiang, E. I., & Goldreich, P. 1997, ApJ, 490, 368

```
Cleeves, L. I., Öberg, K. I., Wilner, D. J., et al. 2016, ApJ, 832, 110
D'Alessio, P., Cantö, J., Calvet, N., & Lizano, S. 1998, ApJ, 500, 411
Draine, B. T., & Lee, H. M. 1984, ApJ, 285, 89
Dullemond, C. P., Dominik, C., & Natta, A. 2001, ApJ, 560, 957
Facchini, S., Birnstiel, T., Bruderer, S., & van Dishoeck, E. F. 2017, A&A,
Flaherty, K. M., Hughes, A. M., Rose, S. C., et al. 2017, ApJ, 843, 150
Gaia Collaboration, Prusti, T., & de Bruijne, J. H. J. 2016, A&A, 595, A1
Gaia Collaboration, Smart, R. L., Sarro, L. M., et al. 2021, A&A, 649, A6
Ginski, C., Stolker, T., Pinilla, P., et al. 2016, A&A, 595, A112
Harries, T. J. 2000, MNRAS, 315, 722
Harries, T. J. 2011, MNRAS, 416, 1500
Harries, T. J., Monnier, J. D., Symington, N. H., & Kurosawa, R. 2004,
Hughes, A. M., Wilner, D. J., Andrews, S. M., Qi, C., & Hogerheijde, M. R.
  2011, ApJ, 727, 85
Hughes, J., Hartigan, P., Krautter, J., & Kelemen, J. 1994, AJ, 108, 1071
Isella, A., Guidi, G., Testi, L., et al. 2016, PhRvL, 117, 251101
Kenyon, S. J., & Hartmann, L. 1987, ApJ, 323, 714
Kraus, S., Kreplin, A., Young, A. K., et al. 2020, Sci, 369, 1233
Lagage, P.-O., Doucet, C., Pantin, E., et al. 2006, Sci, 314, 621
Lucy, L. B. 1999, A&A, 344, 282
Malbet, F., & Bertout, C. 1991, ApJ, 383, 814
Manoj, P., Bhatt, H. C., Maheswar, G., & Muneer, S. 2006, ApJ, 653, 657
Meyer, F., & Meyer-Hofmeister, E. 1982, A&A, 106, 34
Monnier, J. D., Harries, T. J., Aarnio, A., et al. 2017, ApJ, 838, 20
Montesinos, M., Cuello, N., Olofsson, J., et al. 2021, ApJ, 910, 31
Müller, H. S. P., Schlöder, F., Stutzki, J., & Winnewisser, G. 2005, JMoSt,
Natta, A., Prusti, T., Neri, R., et al. 2001, A&A, 371, 186
Panić, O., Hogerheijde, M. R., Wilner, D., & Qi, C. 2009, A&A, 501, 269
Pinte, C., Ménard, F., Duchêne, G., et al. 2018, A&A, 609, A47
Podio, L., Garufi, A., Codella, C., et al. 2020, A&A, 642, L7
Pohl, A., Benisty, M., Pinilla, P., et al. 2017, ApJ, 850, 52
Rich, E. A., Wisniewski, J. P., Currie, T., et al. 2019, ApJ, 875, 38
Rich, E. A., Wisniewski, J. P., Sitko, M., & Grady, C. 2020, ApJ, 902, 4
Rundle, D., Harries, T. J., Acreman, D. M., & Bate, M. R. t. 2010, MNRAS,
  407, 986
Schöier, F. L., van der Tak, F. F. S., van Dishoeck, E. F., & Black, J. H. 2005,
   A&A, 432, 369
Teague, R. 2019, JOSS, 4, 1632
Teague, R., Bae, J., Bergin, E. A., Birnstiel, T., & Foreman-Mackey, D. 2018,
   ApJL, 860, L12
van den Ancker, M. E., de Winter, D., & Tjin A Djie, H. R. E. 1998, A&A,
  330, 145
Villenave, M., Ménard, F., Dent, W. R. F., et al. 2020, A&A, 642, A164
Vioque, M., Oudmaijer, R. D., Baines, D., Mendigutía, I., &
  Pérez-Martínez, R. 2018, A&A, 620, A128
Walsh, C., Juhász, A., Meeus, G., et al. 2016, ApJ, 831, 200
Wichittanakom, C., Oudmaijer, R. D., Fairlamb, J. R., et al. 2020, MNRAS,
  493, 234
Williams, J. P., & Best, W. M. J. 2014, ApJ, 788, 59
Wisniewski, J. P., Clampin, M., Grady, C. A., et al. 2008, ApJ, 682, 548
Yang, B., Stancil, P. C., Balakrishnan, N., & Forrey, R. C. t. 2010, ApJ,
  718, 1062
```